



HAL
open science

A synergetic approach for estimating the local direct aerosol forcing: Application to an urban zone during the Expérience sur Site pour Contraindre les Modèles de Pollution et de Transport d'Emission (ESCOMPTE) experiment

Jean-Claude Roger, M. Mallet, P. Dubuisson, H. Cachier, E. Vermote, O. Dubovik, S. Despiiau

► **To cite this version:**

Jean-Claude Roger, M. Mallet, P. Dubuisson, H. Cachier, E. Vermote, et al.. A synergetic approach for estimating the local direct aerosol forcing: Application to an urban zone during the Expérience sur Site pour Contraindre les Modèles de Pollution et de Transport d'Emission (ESCOMPTE) experiment. Journal of Geophysical Research, 2006, 111, pp.D13208. 10.1029/2005JD006361 . hal-00138869

HAL Id: hal-00138869

<https://hal.science/hal-00138869>

Submitted on 30 Oct 2020

HAL is a multi-disciplinary open access archive for the deposit and dissemination of scientific research documents, whether they are published or not. The documents may come from teaching and research institutions in France or abroad, or from public or private research centers.

L'archive ouverte pluridisciplinaire **HAL**, est destinée au dépôt et à la diffusion de documents scientifiques de niveau recherche, publiés ou non, émanant des établissements d'enseignement et de recherche français ou étrangers, des laboratoires publics ou privés.

A synergetic approach for estimating the local direct aerosol forcing: Application to an urban zone during the Expérience sur Site pour Contraindre les Modèles de Pollution et de Transport d'Emission (ESCOMPTE) experiment

J. C. Roger,^{1,2,3} M. Mallet,⁴ P. Dubuisson,³ H. Cachier,⁵ E. Vermote,¹ O. Dubovik,² and S. Despiou⁶

Received 12 June 2005; revised 25 January 2006; accepted 17 March 2006; published 15 July 2006.

[1] A method dedicated to the investigation of direct radiative forcing of the main anthropogenic aerosol species (ammonium sulfate, black carbon, particulate organic matter) is presented. We computed the direct radiative aerosol forcing at the top of atmosphere (TOA), at the bottom of atmosphere (BOA), and into the atmospheric layer (ATM). The methodology is based on chemical, photometric, and satellite measurements. We first determined the optical properties of the main aerosol species and then computed their direct radiative impact at local scale. The method was applied to a periurban zone during the Expérience sur Site pour Contraindre les Modèles de Pollution et de Transport d'Emission experiment. Optical computations indicate that the single scattering albedo, for the total aerosol population in the external mixture, is equal to 0.83 ± 0.04 at 550 nm, indicative of a strong absorption of the solar radiation. At the same time the mean asymmetry parameter is equal to 0.59 ± 0.04 , and the mean aerosol optical thickness is equal to 0.30 ± 0.02 , at 550 nm. The anthropogenic urban aerosol layer reduces significantly the daily surface illumination ($-24 \text{ W m}^{-2} > \Delta F_{\text{BOA}} > -47.5 \text{ W m}^{-2}$) by reflection to space ($-6 \text{ W m}^{-2} > \Delta F_{\text{TOA}} > -9 \text{ W m}^{-2}$) and by absorption of the solar radiation into the atmosphere ($17 \text{ W m}^{-2} < \Delta F_{\text{ATM}} < 39 \text{ W m}^{-2}$). The available resulting energy in the atmospheric column heats the lowermost part of the atmosphere from 1.1°K d^{-1} to 2.8°K d^{-1} . Our study shows that the black carbon particles have a large contribution to the BOA forcing (almost 50% of the total daily forcing), whereas the ammonium sulfate particles contribute only to about 10%. Conversely, the TOA daily forcing is mostly driven by the ammonium sulfate aerosol (around 50%).

Citation: Roger, J. C., M. Mallet, P. Dubuisson, H. Cachier, E. Vermote, O. Dubovik, and S. Despiou (2006), A synergetic approach for estimating the local direct aerosol forcing: Application to an urban zone during the Expérience sur Site pour Contraindre les Modèles de Pollution et de Transport d'Emission (ESCOMPTE) experiment, *J. Geophys. Res.*, *111*, D13208, doi:10.1029/2005JD006361.

1. Introduction

[2] The aerosol direct radiative effect represents, at this time, one of the largest sources of uncertainty in estimating regional climate changes [Haywood and Boucher, 2000; Intergovernmental Panel on Climate Change, 2001]. To

reduce these uncertainties, numerous experimental campaigns were performed for different aerosol regimes. Hignett *et al.* [1999] and Russell *et al.* [1999] reported estimations of the direct forcing during TARFOX [Hobbs, 1999] for anthropogenic aerosols transported from the United States eastern seaboard. Bush and Valero [2002], Léon *et al.* [2002], Satheesh and Ramanathan [2000] and Satheesh *et al.* [1999] estimated the direct forcing during the Indian Ocean Experiment (INDOEX) [Ramanathan *et al.*, 2001], for anthropogenic aerosols transported from the Indian continent. Markowicz *et al.* [2003] reported simulations of the direct forcing exerted by the aerosol pollution on the Mediterranean Sea during MINOS [Lelieveld *et al.*, 2002]. Finally, Markowicz *et al.* [2003], Bush and Valero [2003], and Nakajima *et al.* [2003] simulated an estimation of the aerosol direct radiative effect during the ACE-Asia campaign [Huebert *et al.*, 2003]. At the global scale, remote sensing of aerosol optical characteristics has made consid-

¹Department of Geography, University of Maryland at College Park, College Park, Maryland, USA.

²NASA Goddard Space Flight Center, Greenbelt, Maryland, USA.

³Ecosystèmes Littoraux aux Côtiers, Université du Littoral Côte d'Opale, Wimereux, France.

⁴Laboratoire d'Aérodologie, Observatoire Midi-Pyrénées, Toulouse, France.

⁵Laboratoire des Sciences du Climat et l'Environnement, CEA/CNRS, Gif-sur-Yvette, France.

⁶Laboratoire des Echanges Particulaires aux Interfaces, Université de Toulon et du Var, La Garde, France.

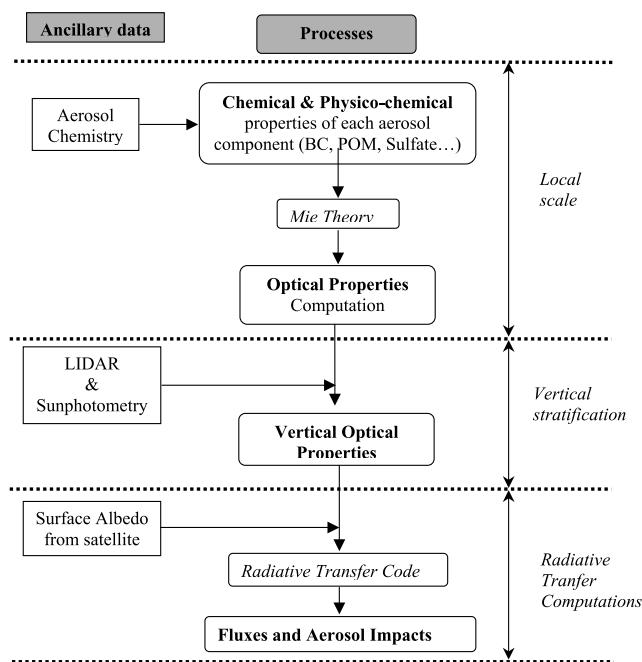


Figure 1. Methodology used.

erable progress with the last generation of satellites (see King *et al.* [1999] for an overview and Tanré *et al.* [1999] as an example of MODIS) and can be useful for climate study [Kaufman *et al.*, 2002].

[3] The purpose of this work is to present a new methodology allowing the determination of the direct aerosol forcing at a local scale. This methodology relies on a synergetic approach using in situ chemical and optical measurements of the aerosol associated with integrated measurements (Sun photometer, LIDAR, airborne and satellite measurements) and a radiative transfer code which gives access to the direct forcing for the different aerosol components [Dubuisson *et al.*, 1996].

[4] Optical properties of the aerosol (extinction and scattering coefficients, asymmetry factor) have been retrieved from particle size distribution and chemical characterization in each class bin [Mallet *et al.*, 2003]. The vertical stratification of optical properties is resolved, provided some hypothesis on the aerosol composition and using aircraft particle profiles. Surface albedo is obtained from satellite measurements [Vermote *et al.*, 2002]. Important constrains are provided at each step by sky and sun photometry [Holben *et al.*, 1998] and LIDAR measurements. Finally, the atmospheric radiation fluxes are computed at each altitude.

[5] This methodology is applied to an urban aerosol, for which the climatic effect is not well known at the present time. Indeed, among all the numerous sources of anthropogenic aerosol particles, the pollutant particles emitted in large urban areas are now clearly recognized as one of the most important and cities emerge as an important research topic in atmospheric chemistry and effect on climate. Particulate pollutants emitted in industrialized regions, mainly consist of sulfate, nitrate, black carbon and particulate organic matter. The particles modify the albedo of the surface-atmosphere system, leading to a modification of the

local or regional climate when pollutants are transported out of the source regions.

[6] Results presented hereafter are focused on the local daily direct radiative forcing exerted by anthropogenic aerosols generated during strong pollution events occurring during the Expérience sur Site pour Contraindre les Modèles de Pollution et de Transport d’Emission (ESCOMPTE) experiment [Cros *et al.*, 2004; Cachier *et al.*, 2005].

2. Methodology to Compute the Aerosol Radiative Forcing

2.1. Experimental Campaign: Expérience sur Site pour Contraindre les Modèles de Pollution et de Transport d’Emission (ESCOMPTE)

[7] Between 4 June and 13 July 2001, the ESCOMPTE program was devoted to producing a relevant set of data for testing and evaluating regional pollution models [Cros *et al.*, 2004]. The field campaign took place, over an area of 100 km × 100 km, in a southeastern part of France including the urban area of the city of Marseille (1.2 million inhabitants), the Rhône valley and the large industrial complex of Fos-Berre. Owing to urban and industrial emissions, and the strong solar radiation, high and frequent pollution events are regularly observed in this area (O₃ peaks for example).

[8] The physical and chemical characterization of aerosol particles [Cachier *et al.*, 2005] was among the numerous objectives of this experiment. Measurements were mainly carried out during intensive observation periods (IOPs), which correspond to meteorological conditions favorable to pollution events, which can be summarized as follows: (1) anticyclonic conditions; (2) coastal breeze; and (3) strong solar radiation leading to high temperatures (25°–30°C). From the data set, we use all days for which aerosol optical and chemical measurements were available. Thus 5 days are selected to estimate the direct radiative effect of the anthropogenic particles (POI 2b, 24–26 June, and POI 3, 2–3 July) based on a data set measured in the periurban zone, called the “Vallon Dol” site, located 2 km north of Marseille, and mainly polluted by the urban traffic.

2.2. Aerosol Optical Properties

[9] The aim of the present method is to combine chemical and optical characterizations, as shown Figure 1. During ESCOMPTE, the particles optical properties were determined using impactors. This determination was described in detail by Mallet *et al.* [2003] and only the general principles are given here. The work starts with the ionic chromatography and the analysis of the carbon by a multistep thermal method [Putaud *et al.*, 2000] from which the mass size distributions of aerosol species are determined (black carbon (BC), particulate organic matter (POM), ammonium sulfate (AS), nitrate (N), sea salt (SS), and dust (D) are selected as optical species (see Figure 2)). The size distributions are represented by two different modes, i.e., the accumulation mode (submicrometric) and the coarse mode (supermicrometric) respectively indexed in the following by “a” and “c.” In practice, the two distributions are fitted with a lognormal function, from which the standard deviation σ and the “mass” mode radius $r_{g,m}$ are retrieved, the latter being transformed into “number” distribution param-

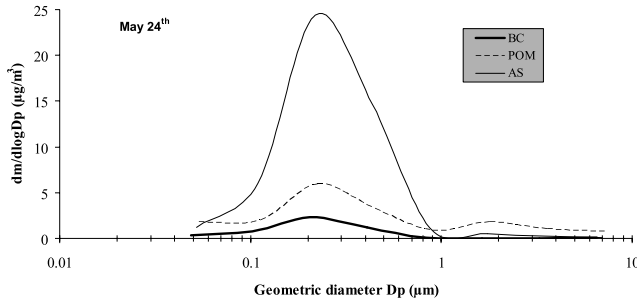


Figure 2. Example of mass size distribution used (acquired on 24 May).

eters $r_{g,n}$ [Seinfeld and Pandis, 1998]. For each aerosol component, the complex refractive index m was selected based on previously published studies. These microphysical properties are all reported (Table 1) for the major aerosol species encountered during the ESCOMPTE experiment (BC, AS, POMa and POMc). The dependence of the aerosol properties with the relative humidity RH (mean daily values are given in Table 2) is computed using the H \ddot{a} nel's [1976] relation. Then, assuming spherical particles, the spectral optical properties are spectrally computed using the Mie theory [Mie, 1908] to derive the extinction coefficient $K_{\text{ext}}(\lambda)$, the scattering coefficient $K_{\text{sca}}(\lambda)$, the absorption coefficient $K_{\text{abs}}(\lambda)$ (with $K_{\text{ext}}(\lambda) = K_{\text{sca}}(\lambda) + K_{\text{abs}}(\lambda)$) and the asymmetry factor $g(\lambda)$, where λ is the wavelength. In the following sections, we also use the single scattering albedo $\omega_o(\lambda)$ ($=K_{\text{sca}}(\lambda)/K_{\text{ext}}(\lambda)$). These optical properties are reported in Table 2 at 550 nm for the major aerosol species given above.

2.3. Vertical Stratification

[10] The second step is to establish the stratification of the aerosol optical properties for the vertical dimension. For that purpose, we split the atmosphere into four major layers: (1) surface to urban boundary layer (UBL) (low troposphere); (2) UBL to aircraft altitude (mean troposphere); (3) aircraft altitude to tropopause (free troposphere); and (4) tropopause to stratopause (stratosphere). The first layer corresponds to the low troposphere (LT), between the surface and the top of the UBL, which is around 1 km high during ESCOMPTE. This layer was very stable during the pollution events, and the mixing of the particles is assumed homogeneous (this point has been confirmed by the modeling group). The second atmospheric layer is the mean troposphere (MT), between 1 and 3 km where LIDAR

measurements were performed. Finally, we distinguish the free troposphere (FT) and the stratosphere (ST).

[11] Regarding thermodynamical parameters, vertical soundings acquired from the French Airplane for Remote Sensing and Atmospheric Research (ARAT) [van Dingenen *et al.*, 2002] are used for temperature, relative humidity, ozone concentration, and particle number (from 0 to 3 km, including the LT and MT layers) as shown Figure 3. We complete the stratification for FT and ST with climatology data (midlatitude summer).

[12] Following the scheme used in the radiative transfer code Global Atmospheric Model (GAME) (section 2.4), these four major layers are sliced into 33 levels. The aerosol optical properties computed from the in situ measurements are used for both for the layers LT and MT accounting for the sedimentation of the aerosol coarse mode into MT. For FT and ST, we use optical properties coming from the free tropospheric and stratospheric aerosol models described by Hess *et al.* [1998]. Moreover, according to Mallet *et al.* [2004], there is no need to consider aerosols transported from remote sources (such as desert aerosols) at Vallon Dol during the studied POI. Thus each 33 levels are filled up with the thermodynamical parameters (pressure, temperature), the number of each component N_i and the aerosol optical properties ($K_{\text{ext}}(\lambda)$, $g(\lambda)$, $\omega_o(\lambda)$).

[13] We start by adjusting the number of particles of the LT layer (assumed homogenous). The constraint we used is the spectral aerosol optical thicknesses $\delta_a^{\text{AERONET}}(\lambda)$ measured by the PHOTON/AERONET network [Holben *et al.*, 1998]. We assume that $\delta_a^{\text{AERONET}}(\lambda)$ should be equal to $\delta_a^*(\lambda)$ with

$$\delta_a^*(\lambda) = \sum_{n=1}^{33} \left(\sum_i \frac{N_i(z)}{N(z)} K_{\text{ext}}^i(\lambda, n) \right) \Delta z(n). \quad (1)$$

[14] To complete the vertical stratification, we need the surface albedo, which is a critical parameter in the estimation of the top of atmosphere direct radiative forcing. Indeed, according Bergstr \ddot{o} m and Russell [1999], the aerosol forcing at the top of the atmosphere can be either positive or negative depending of the surface albedo value (with a critical rocking value around 0.3 at 550 nm). We estimate the spectral surface albedo from the MODIS surface reflectance product [Vermote *et al.*, 2002] generated from data collected by the TERRA platform (averaged over a 3 km \times 3 km area). In our case of a suburban environment, we find low values (Figure 4) far from the rocking value.

Table 1. Mean Microphysical (Radius $r_{g,n}$, Variance σ , and Dry Refractive Index m) and Optical (Extinction Coefficient K_{ext} , Single Scattering Albedo ω_o , and Asymmetry Factor g) Properties at 550 nm for the Most Important Species^a

	All Species	BC	POMa ^b	POMc ^b	AS
$r_{g,n}$		0.028 \pm 0.010	0.034 \pm 0.010	0.364 \pm 0.120	0.050 \pm 0.10
Σ		1.94 \pm 0.14	1.86 \pm 0.16	1.95 \pm 0.19	1.74 \pm 0.07
m (dry)		1.87 – 0.569 <i>i</i>	1.55 – 0.005 <i>i</i>	1.55 – 0.005 <i>i</i>	1.53 – 0.006 <i>i</i>
K_{ext}		0.012 \pm 0.004	0.009 \pm 0.004	0.002 \pm 0.001	0.026 \pm 0.010
Ω_o	0.85 \pm 0.03	0.33 \pm 0.03	0.98 \pm 0.01	0.94 \pm 0.01	0.97 \pm 0.01
G	0.59 \pm 0.02	0.43 \pm 0.04	0.59 \pm 0.06	0.74 \pm 0.01	0.58 \pm 0.01

^aSee Mallet *et al.* [2003].

^bPOMa is the accumulation mode; POMc is the coarse mode.

Table 2. Mean Aerosol Optical Properties Computed at 550 nm and Daily Direct Radiative Forcing for the Total Aerosol Population During POI 2 and 3

	24 Jun	25 Jun	26 Jun	2 Jul	3 Jul
δa^a	0.31	0.41	0.25	0.28	0.21
Ω_o	0.86	0.82	0.81	0.84	0.85
G	0.60	0.62	0.60	0.57	0.58
Relative humidity, %	61.4	61.0	45.0	45.0	55.0
<i>Daily Direct Radiative Forcing ΔF ($W m^{-2}$)</i>					
BOA	-35.5	-47.6	-31.1	-33.3	-23.9
TOA	-9.1	-8.5	-6.1	-8.2	-6.5
ATM	26.4	39.1	25.0	25.1	17.4

^aVariable δa represents the aerosol optical thickness over the atmospheric column at 550 nm.

2.4. Radiative Transfer Computations and Conventions Used

[15] The direct aerosol radiative forcing at bottom of atmosphere (BOA), at top of atmosphere (TOA), and into the atmospheric layer (ATM) are computed using the radiative transfer model GAME [Dubuisson *et al.*, 1996], which accounts for the scattering and absorption processes by particles and gases. In this model, the absorption includes the absorbers in the short-wave region and is based on the results of a line by line code [Scott, 1974]. Multiple scattering effects are treated using the discrete ordinates method (DOM) [Stamnes *et al.*, 1988] following the plane-parallel approximation. This method allows accurate treatment of scattering and absorption by aerosols, clouds and molecules. The DOM employs a Legendre polynomial decomposition for the phase function and the radiance. Interactions between multiple scattering and gaseous absorption are accurately treated using the correlated- k method [Lacis and Oinas, 1991].

[16] Upward and downward net radiative fluxes F are computed over the spectral solar range (integrated from 0.3 μm to 3.0 μm) for each of the 33 levels of the atmosphere. From these fluxes, the daily direct forcing at

the bottom of the atmosphere, ΔF_{BOA} , and at the top of the atmosphere, ΔF_{TOA} , are defined by

$$\Delta F_{BOA} = F_{BOA}^w - F_{BOA}^o \quad \Delta F_{TOA} = -(F_{TOA}^w - F_{TOA}^o), \quad (2)$$

respectively, where F^w and F^o are the net fluxes with and without aerosols, respectively. With this convention, a negative sign of the daily ΔF implies an aerosol cooling effect.

[17] Through absorption and scattering, the aerosols decrease the energy reaching the surface ($F_{BOA}^w < F_{BOA}^o$). At the top of the atmosphere, the aerosols increase the reflectivity of the atmosphere ($F_{TOA}^w > F_{TOA}^o$). Thus more energy is “reflected” by the Earth-atmosphere system, and less energy is available for the Earth-atmosphere system, inducing in a cooling at TOA

[18] The direct atmospheric forcing, ΔF_{ATM} , is defined as

$$\Delta F_{ATM} = \Delta F_{TOA} - \Delta F_{BOA}. \quad (3)$$

In the case of pure scattering aerosol ($\omega_o = 1$), ΔF_{ATM} is equal to zero. The presence of aerosols contributes to a loss of energy at the surface level, this lost energy being scattered upward to space. In a case of an absorbing aerosol ($\omega_o < 1$), a part of this loss at the surface level is absorbed into the atmospheric layer. The increase in energy in the atmospheric layers leads to a heating of these layers.

[19] To get an idea of the importance of the impact, we computed the vertical profile of the heating rate given at an atmospheric altitude z as by

$$\frac{\partial T}{\partial t} = -\frac{1}{\rho C_p} \frac{\partial F(z)}{\partial z}, \quad (4)$$

where T is the radiative temperature of the air, ρ is the air density, C_p is the specific heat of the air, and $F(z)$ is the net flux at the altitude z .

3. Daily Direct Forcing due to Anthropogenic Particles

[20] One advantage of the present method is that it provides the daily direct aerosol forcing at each altitude

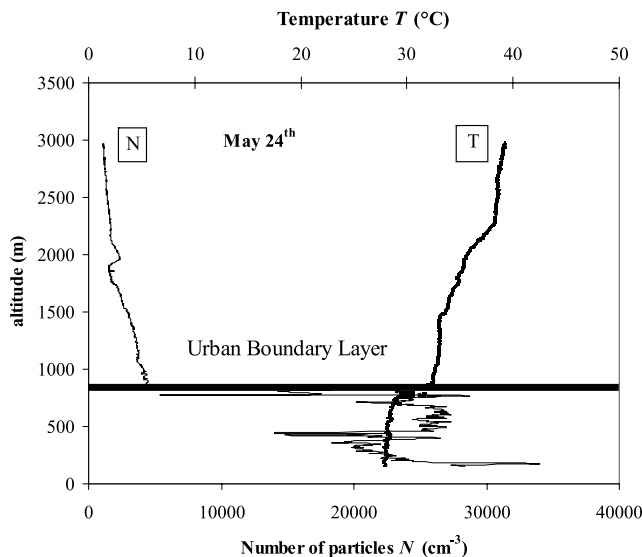


Figure 3. Example of vertical profiles used for the number of particles and the temperature (acquired on 24 May).

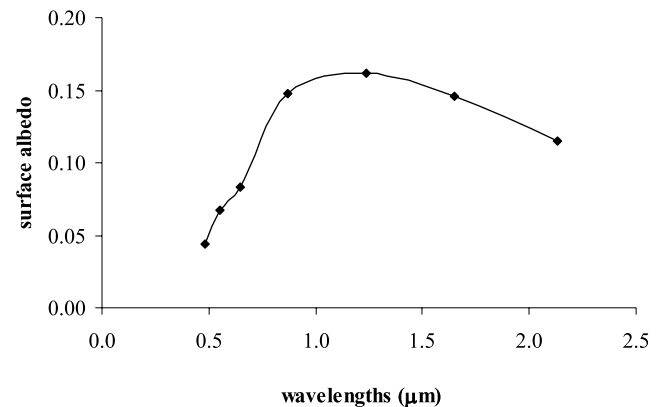


Figure 4. Surface albedo over the site “Vallon Dol” from EOS/MODIS data.

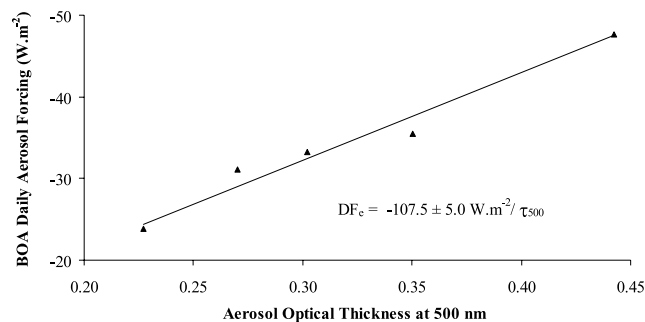


Figure 5. Bottom of atmosphere (BOA) daily aerosol forcing versus the aerosol optical thickness at 500 nm and daily forcing efficiency DFe.

for the aerosol mixing and for each of its components. In a previous study at the Vallon Dol site [Mallet et al., 2004], we have shown that the mixing state of aerosols during the experiment could be considered as externally based on the values of the single scattering albedo retrieved by PHOTON/AERONET photometers measurements [Dubovik et al., 2002].

[21] Results of the daily direct solar spectrum forcing due to anthropogenic particles during ESCOMPTE are presented in Table 2. At surface (BOA), we find negative fluxes, which imply a cooling effect. The daily direct forcing ranges from -24.0 W m^{-2} to -47.5 W m^{-2} for an aerosol optical thickness δ_a ranging from about 0.2 to 0.4 at 500 nm (see Table 2). The daily surface forcing efficiency (defined here by the daily surface forcing divided by δ_a at 500 nm) is $DFe = -107.5 \text{ W m}^{-2}$ at 500 nm (Figure 5), which is on the higher end of the range of values reported in the literature. Indeed, for the INDOEX experiment, several authors [Satheesh et al., 1999; Satheesh and Ramanathan, 2000; Ramanathan et al., 2001; Léon et al., 2002; Bush and Valero, 2002] have found a value of DFe equal to about -75 W m^{-2} . This value is almost the same as those found during TARFOX [Hobbs, 1999; Russell et al., 1999; Hignett et al., 1999] and ACE-ASIA [Bush and Valero, 2003; Nakajima et al., 2003] (-70 W m^{-2} to -75 W m^{-2}). This high value of the daily forcing efficiency can be explained by the fact that the urban aerosols observed during ESCOMPTE exert a greater absorption in the atmosphere

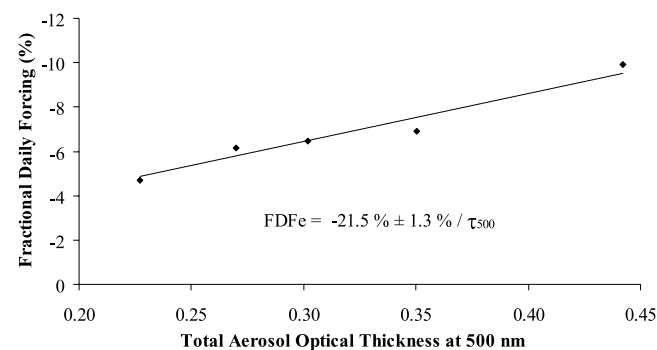


Figure 6. Same as Figure 5, but for the fractional daily forcing and fractional daily forcing efficiency FDFe.

and a lower backscattering to space mainly due to a high black carbon concentration [Cachier et al., 2005; Mallet et al., 2003]. The aerosol single scattering during ESCOMPTE was about 0.85 at 550 nm, instead of 0.90 and 0.93 respectively during INDOEX and TARFOX.

[22] The large absorption by the atmosphere is also observed with the fractional daily forcing (defined by Bush and Valero [2003] as being the BOA forcing divided by the TOA flux). We find an efficiency FDFe of -21.5% at 500 nm (Figure 6), meaning a high capability for the atmosphere to force the incident solar radiation (Bush and Valero [2003] reported -18% and -16.8% respectively for ACE-Asia and INDOEX). These fractional forcings are directly associated here with a strong positive daily atmospheric forcing ΔF_{ATM} (from $+17.5 \text{ W m}^{-2}$ to $+39.0 \text{ W m}^{-2}$), leading to a heating rate reaching 2.5°K d^{-1} and 1°K d^{-1} at surface for the heaviest and lightest condition of pollution, respectively. Finally, the forcing ΔF_{TOA} at the top of the atmosphere corresponds (Table 2) to a cooling, but with an order of magnitude four times less than at the surface (from -6.0 W m^{-2} to -9.0 W m^{-2}). This result again indicates an important amount of energy absorbed into the atmosphere.

[23] As an example, the aerosol radiative impact produced by each major atmospheric layer is reported in Figure 7 for 25 June. For upwelling and downwelling fluxes, the aerosol impact takes place under the urban boundary layer; the rest of the atmosphere only contributes for about 5%. This repartition is normal given the fact that most of the aerosols were located under the UBL [Mallet et al., 2003]. Consequently, the heating of the atmosphere due to aerosols is located to the lowermost part of the atmosphere (under the UBL), as shown in Figure 8 for two extreme conditions of pollution.

4. Contribution of Each Aerosol Species to the Direct Forcing

[24] Tables 3, 4, and 5 present, for each aerosol species, respectively the daily direct radiative forcing at the surface level ΔF_{BOA} , at the top of the atmosphere ΔF_{TOA} , and into the atmosphere ΔF_{ATM} . We present the main aerosol components (black carbon, ammonium sulfate and particulate organic matter).

[25] At the surface, about 90% of ΔF_{BOA} (Table 3) is due to anthropogenic aerosols. Simulations indicate the crucial role of black carbon particles, which contribute for 50% to

Atmospheric Layer	$\Delta F_{\downarrow}(\text{layer})$	ΔF_{\downarrow}	$\Delta F_{\uparrow}(\text{layer})$	ΔF_{\uparrow}
Stratosphere	-0.2	0 W.m^{-2} -47.6 W.m^{-2}	-0.1	-8.5 W.m^{-2} $+4.5 \text{ W.m}^{-2}$
Free Troposphere	-0.7		-0.1	
Mean Troposphere	-1.0		-0.4	
Low Troposphere	-45.6		-12.4	
Surface	-47.6		-47.6	

Figure 7. Contribution of each atmospheric layer to the daily aerosol direct impact (downward and upward): example of 25 June.

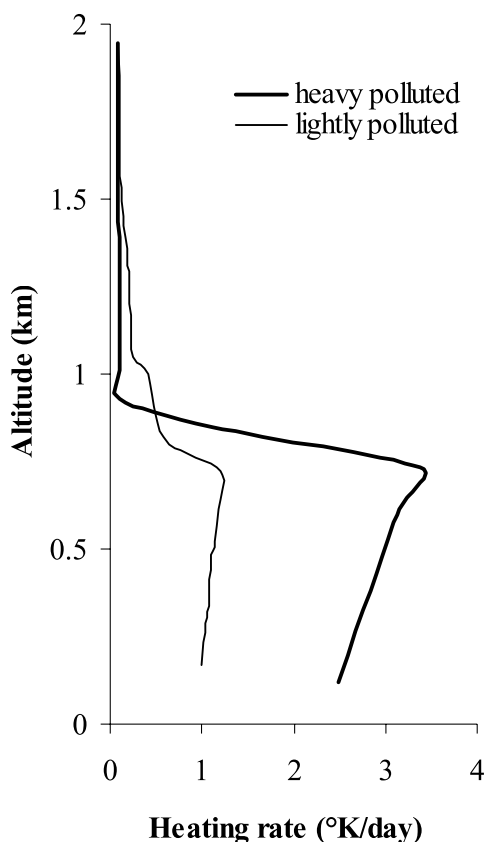


Figure 8. Vertical heating rate computed for two atmospheric situations.

ΔF_{BOA} . The daily direct radiative forcing at surface of the black carbon is about twice as large as the one exerted by the ammonium sulfate. This result totally agrees with observations made during INDOEX by *Satheesh and Ramanathan* [2000], which indicates that black carbon is the main contributor to the light attenuation at surface. A second interesting point is the fact that the black carbon scattering drives the forcing at surface in a higher order of magnitude than the ammonium sulfate (Figure 9), while the black carbon absorption directly infers the atmospheric forcing (Figure 10). Finally, the contribution of the particulate organic matter (a little less than 15%) needs to be considered, mainly due to the accumulation mode which is optically more efficient in scattering and absorbing light in the visible range than the coarse mode [Mallet *et al.*, 2003].

[26] At the top of the atmosphere (Table 4), the ammonium sulfate and the particulate organic matter aerosols

Table 3. Aerosol Daily Direct Surface Forcing ΔF_{BOA} for the Main Aerosol Pollutants^a

	BC	POMa ^b	POMc ^b	AS
24 Jun	-15.5	-3.0	-0.5	-10.0
25 Jun	-24.0	-4.0	-1.0	-10.0
26 Jun	-15.0	-3.5	-1.0	-6.0
2 Jul	-14.0	-3.0	-1.0	-9.0
3 Jul	-9.5	-2.5	-0.5	-6.5

^aUnits are W m^{-2} .

^bPOMa is the accumulation mode; POMc is the coarse mode.

Table 4. Aerosol Daily Direct Top of Atmosphere Forcing ΔF_{TOA} for the Main Aerosol Pollutants^a

	BC	POMa ^b	POMc ^b	AS
24 Jun	+2.5	-2.0	-0.5	-6.5
25 Jun	+3.5	-2.5	-0.5	-5.0
26 Jun	+2.0	-2.0	-0.5	-3.0
2 Jul	+2.0	-2.0	-0.5	-5.0
3 Jul	+1.0	-1.5	-0.5	-3.5

^aUnits are W m^{-2} .

^bPOMa is the accumulation mode; POMc is the coarse mode.

exert a cooling effect by reflecting the solar fluxes back to space. Ammonium sulfate is the major contributor and leads to a ΔF_{TOA} forcing twice as large as the particulate organic matter (in agreement with *Ramanathan et al.* [2001]). It should be again noticed that about 90% of the particulate organic matter forcing is due to the accumulation mode. Results also indicate that the black carbon aerosol is the only chemical species inducing a positive forcing. This forcing is due to black carbon's high capability to absorb the solar radiation into the atmosphere.

[27] Concerning the contribution of the different aerosol species to ΔF_{ATM} , all the anthropogenic particles contribute to a positive ΔF_{ATM} (Table 5). ΔF_{ATM} is mainly due to the absorbing black carbon aerosols (about 75% while AS represents 15%). These percentages are almost identical for the heating rate (80 and 10%, respectively). In the worst polluted case (25 June), the black carbon particles produce a heating rate of 2.1°K d^{-1} at the surface. Furthermore, a weak contribution of the particulate organic matter is observed (about 8% for ΔF_{ATM} and for the heating rate).

5. Error Budget

[28] The code GAME used in this study has participated to an intercomparison exercise [*Halothore et al.*, 2005]. The results of this exercise indicated that GAME is accurate to a few units of watt ($1-3$) for a flux reaching 1000 W m^{-2} . The impact of this uncertainty on the forcing estimate should be reduced because we work with relative fluxes integrated over all the day.

[29] The second source of uncertainties comes from the chemical and physicochemical parameters (i.e., mass, density, mean radius in mass, refractive index, etc.) which serve as the basis for our scheme. For each of these parameters, we define an uncertainty based on the observed variability. Thus we apply $\pm 25\%$ on the density, $\pm 10\%$ on the Lognormal size distribution parameters (i.e., the mean radius in mass and the standard deviation), $\pm 5\%$ on the real refractive index and a range from 0.45 to 0.70 on the imaginary

Table 5. Aerosol Daily Direct Atmospheric Forcing ΔF_{ATM} for the Main Aerosol Pollutants^a

	BC	POMa ^b	POMc ^b	AS
24 Jun	+18.0	+1.0	+0.5	+3.5
25 Jun	+27.5	+1.5	+0.5	+5.0
26 Jun	+17.0	+1.5	+0.5	+3.0
2 Jul	+16.0	+1.0	+0.5	+4.0
3 Jul	+10.5	+1.0	+0.5	+3.0

^aUnits are W m^{-2} .

^bPOMa is the accumulation mode; POMc is the coarse mode.

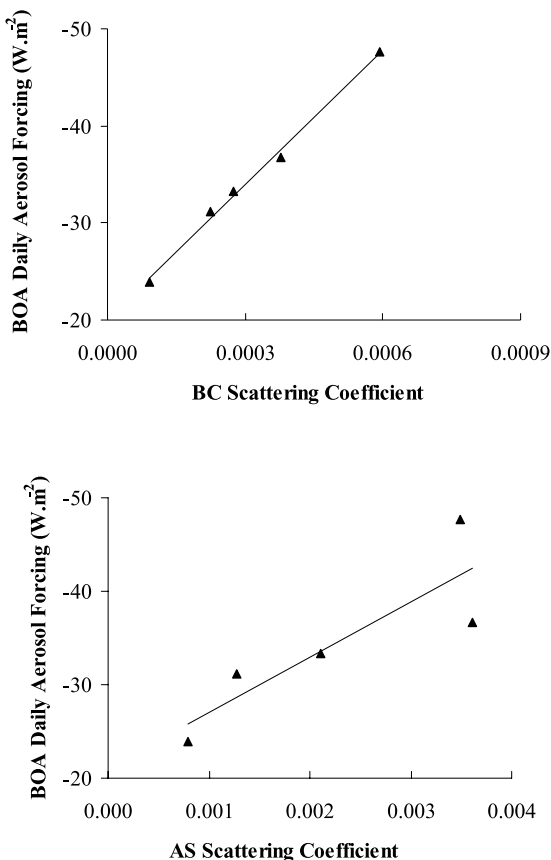


Figure 9. Relationship between the BOA daily aerosol forcing and the scattering coefficient of the black carbon and ammonium sulfate particles.

refractive index of the black carbon. For the mass, we use different percentage according to the methodology used: (1) for aerosol component derived from ionic chromatography (e.g., sulfates), we used $\pm 30\%$ (10% for the sampling on filters and 20% for chemical analyses); (2) for carbonaceous

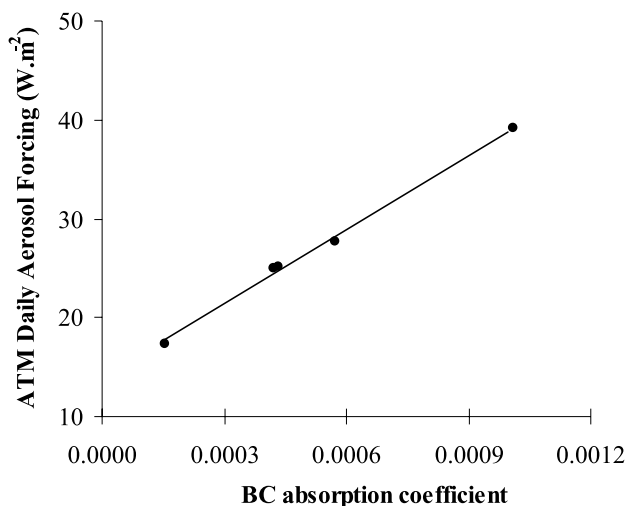


Figure 10. Relationship between the atmospheric (ATM) daily aerosol forcing and the absorption coefficient of the black carbon.

Table 6. Error Budget on the Determination of the Aerosol Daily Forcing Including Physicochemical Parameters of Aerosols^a

	BOA, %	TOA, %	ATM, %
Black carbon			
Refractive index ($\pm 5\%$, $j \pm 25\%$)	∓ 4.0	± 4.0	± 4.0
Mass determination ($\pm 50\%$)	∓ 10.0	± 15.0	± 10.0
Density ($\pm 25\%$)	± 8.0	∓ 10.0	∓ 7.0
Size distribution determination ($\pm 10\%$)	± 7.5	∓ 10.0	∓ 10.0
Sulfate			
Refractive index ($\pm 5\%$)	± 5.0	∓ 11.0	∓ 7.0
Mass determination ($\pm 30\%$)	± 3.0	∓ 4.0	∓ 3.0
Size distribution determination ($\pm 10\%$)	∓ 8.0	± 3.0	± 10.0
POM			
Refractive index ($\pm 5\%$)	± 1.5	∓ 2.0	∓ 0.5
Mass determination ($\pm 80\%$)	± 5.0	∓ 8.0	∓ 4.0
Size distribution determination ($\pm 10\%$)	∓ 2.0	± 0.5	± 2.0
Radiative transfer code	$\leq \pm 0.5$	$\leq \pm 0.5$	$\leq \pm 0.5$
Surface albedo ($\pm 30\%$)	± 1.0	± 15.0	± 4.5
Total	12	20	16

^aIn parentheses the error is considered as input.

components, we used 10% for the sampling on filters and 40% for the chemical analyses, i.e., 50%, with 30% more for POM due to the OC/POM conversion factor in order to account for other atoms than carbon in the organic species. Thus we used $\pm 50\%$ for BC and $\pm 80\%$ for POM. The last source of error is the accuracy of the estimated surface albedo, which mostly impacts the TOA and ATM fluxes. We used satellite data set from EOS/MODIS to estimate this parameter, and we apply a $\pm 30\%$ error on the spectral surface albedo.

[30] Results of induced uncertainties are given in percentage in Table 6. At the end, the overall interpretation of all these uncertainties needs to account for the linked errors and counterbalancing effects. Indeed, if, as an example, we increase the density of BC, then we also have to increase its value of the real refractive index, and according to the sign of the two errors, we need to counterbalance them. Consequently, we can reasonably consider that the daily radiative impacts of aerosols are defined with an accuracy of 12–20% with a better one for BOA in regard of ATM and TOA. These values should be reduced in the future by improving the experimental scheme. Indeed, most of the BOA uncertainties are coming from the physicochemical parameters, but it should be possible to reduce them by applying constraints on the optical ground-based measurements (with aethalometer, nephelometer).

6. Comparison to Ground-Based Measurements and Discussions

[31] As part of the initial validation of this methodology we compared the computed downward fluxes and those measured at the surface. Figure 11 shows an example for 25 June. The agreement between measurements and computations is within 5%.

[32] We then estimated the daily forcing efficiency (at 500 nm) from the measured fluxes at surface (Figure 12). We found a value of $-102.9 \pm 10.0 \text{ W m}^{-2}$, which is in good agreement with the one derived from the computed daily values, $-111.3 \pm 8.0 \text{ W m}^{-2}$ (Figure 13) and the one directly derived from the aerosol forcing, $-107.5 \pm 5.0 \text{ W m}^{-2}$ (Figure 5). These comparisons confirm the validity of the methodology and the error budget.

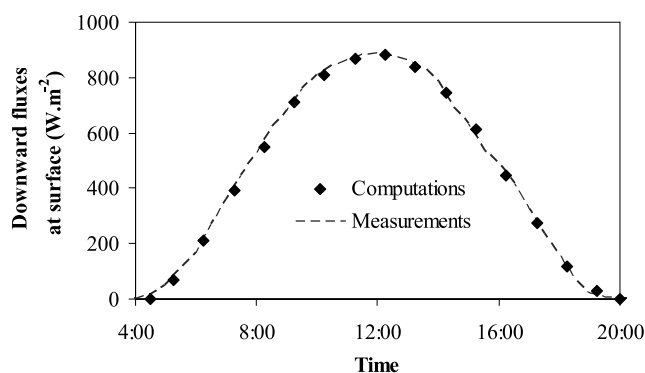


Figure 11. Comparisons between the computed and measured downward fluxes at surface for 25 June.

[33] We also investigated the case of an internal mixing state. Indeed, numerous studies indicated that the different aerosol species are often found in an external mixture close to the pollution source [Hasegawa and Ohta, 2002; van Dingenen et al., 2002]. As already shown by Mallet et al. [2004], the mixture in this data set is close to an external mixing.

[34] In a internal mixture scenario, the asymmetry factor is unchanged, but $\omega_o(\lambda)$ is reduced by 15%, increasing the absorption processes. Compared to the external mixture, the surface illumination should be reduced by 25% (due to an increase of 50% of the energy absorbed into the aerosol layer) which will give us a value outside of our error bars and refutes the hypothesis of the pure internal mixing.

7. Conclusion

[35] The purpose of this work is to present a new methodology allowing the determination of the direct aerosol forcing at a local scale. This methodology is based on in situ physical, chemical and optical measurements of the aerosol, associated with integrated measurements and a radiative transfer code which allows the computation of the aerosol direct forcing.

[36] This methodology was applied to an urban aerosol, for which the climatic effect is not still well known at the present time. At the surface, our results showed a decrease

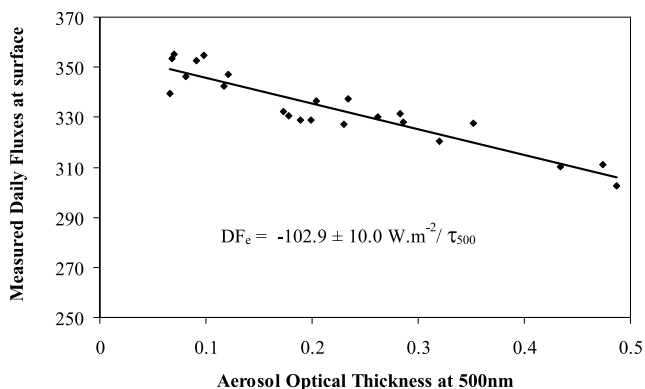


Figure 12. Measured daily fluxes at surface versus the aerosol optical thickness at 500 nm and measured daily forcing efficiency DFe (from 15 June to 9 July).

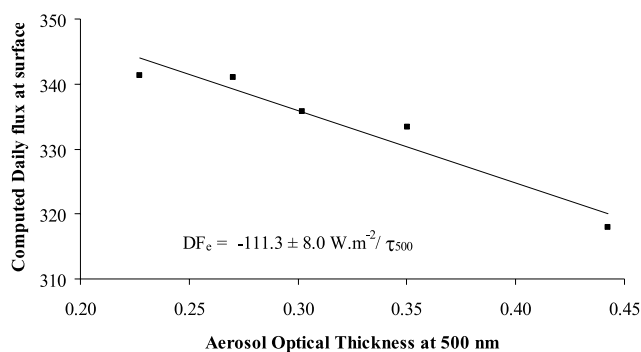


Figure 13. Computed daily fluxes at surface versus the aerosol optical thickness at 500 nm and computed daily forcing efficiency DFe.

of fluxes (negative values of ΔF_{BOA}) meaning a cooling, ranging between -24 W m^{-2} to -47.5 W m^{-2} (with about 12% of accuracy). At the top of the atmosphere, the forcing ΔF_{TOA} was shown to be 4 times lower (from -6 W m^{-2} to -9 W m^{-2} with 20% of accuracy), indicating an important amount of energy absorbed into the atmosphere and then a strong positive daily direct atmospheric forcing ΔF_{ATM} (from $+17.5 \text{ W m}^{-2}$ to $+39 \text{ W m}^{-2}$ with 16% of accuracy).

[37] The study of the contribution of each aerosol species to the direct forcing indicates the crucial role of black carbon particles, which contribute from 50% to ΔF_{BOA} , twice as large as the one exerted by the ammonium sulfate. At the top of the atmosphere, the ammonium sulfate and the particulate organic matter aerosols exert a cooling effect by reflecting the solar fluxes back to space. Ammonium sulfate is the major contributor and leads to a ΔF_{TOA} forcing twice as large as the particulate organic matter. Also, the results indicate that the black carbon aerosol is the only chemical species inducing a positive ΔF_{TOA} . Concerning the contribution of the different aerosol species to ΔF_{ATM} , our study indicates that ΔF_{ATM} is mainly driven by the absorbing black carbon aerosols (about 75% while AS represents 15%).

[38] **Acknowledgments.** The authors are indebted to Bernard Cros and Pierre Durand for the organization of the ESCOMPTE experiment. They gratefully thank the different institutes in France (CNRS, INSU, PNCA, PRIMEQUAL, ADEME, and Ministry of Environment) for their support. Logistic help from local agencies (AIRMAREX and AIRFOBEP) is gratefully acknowledged. We would also like to thank the AERONET/PHOTON staff for the data collection, calibration, and processing and especially the AERONET/PHOTON PIs during ESCOMPTE: P. Goloub (LOA), D. Bahaidin (CIMEL), and D. Tanré (LOA). We also appreciate the data sets provided by J. P. Putaud and R. Van Dingenen from JRC/Ispra (Italy).

References

- Bergström, R. W., and P. B. Russell (1999), Estimation of aerosol direct radiative effects over the mid-latitude North Atlantic from satellite and in situ measurements, *Geophys. Res. Lett.*, *26*, 1731–1734.
- Bush, B. C., and F. P. J. Valero (2002), Spectral aerosol radiative forcing at the surface during the Indian Ocean Experiment (INDOEX), *J. Geophys. Res.*, *107*(D19), 8003, doi:10.1029/2000JD000020.
- Bush, B. C., and F. P. J. Valero (2003), Surface aerosol radiative forcing at Gosan during the ACE-Asia campaign, *J. Geophys. Res.*, *108*(D23), 8660, doi:10.1029/2002JD003233.
- Cachier, H., et al. (2005), Aerosol studies during the ESCOMPTE experiment: An overview, *Atmos. Res.*, *74*, 547–563.
- Cros, B., et al. (2004), An overview of the ESCOMPTE campaign, *Atmos. Res.*, *69*, 3–4, 241–279.

- Dubovik, O., B. N. Holben, T. F. Eck, A. Smirnov, Y. J. Kaufman, M. D. King, D. Tanré, and I. Slutsker (2002), Variability of absorption and optical properties of key aerosol types observed in worldwide locations, *J. Atmos. Sci.*, *59*, 590–608.
- Dubuisson, P., J. C. Buriez, and Y. Fouquart (1996), High spectral resolution solar radiative transfer in absorbing and scattering media: Application to the satellite simulation, *J. Quant. Spectrosc. Radiat. Transfer*, *55*, 103–126.
- Halothore, R. N., et al. (2005), Intercomparison of shortwave radiative transfer codes and measurements, *J. Geophys. Res.*, *110*, D11206, doi:10.1029/2004JD005293.
- Hänel, G. (1976), The properties of atmospheric particles as functions of the relative humidity at thermodynamic equilibrium with surrounding moist air, *Adv. Geophys.*, *19*, 73–188.
- Hasegawa, S., and S. Ohta (2002), Some measurements of the mixing state of soot-containing particles at urban and non-urban sites, *Atmos. Environ.*, *36*, 3899–3908.
- Haywood, J. M., and O. Boucher (2000), Estimates of the direct and indirect radiative forcing due to tropospheric aerosols: A review, *Rev. Geophys.*, *38*(4), 513–543.
- Hess, M., P. Koepke, and I. Schult (1998), Optical properties of aerosols and clouds: The software package, *Bull. Am. Meteorol. Soc.*, *79*, 831–844.
- Hignett, P., J. P. Taylor, P. N. Francis, and M. D. Glew (1999), Comparison of observed and modelled direct forcing during TARFOX, *J. Geophys. Res.*, *104*, 2279–2287.
- Hobbs, P. V. (1999), An overview of the University of Washington airborne measurements and results from the Tropospheric Aerosol Radiative Forcing Observational Experiment (TARFOX), *J. Geophys. Res.*, *104*, 2233–2238.
- Holben, B. N., et al. (1998), AERONET—A federated instrument network and data archive for aerosol characterization, *Remote Sens. Environ.*, *66*, 1–16.
- Huebert, B. J., T. Bates, P. B. Russell, G. Shi, Y. J. Kim, K. Kawamura, G. Carmichael, and T. Nakajima (2003), An overview of ACE-Asia: Strategies for quantifying the relationships between Asian aerosols and their climatic impacts, *J. Geophys. Res.*, *108*(D23), 8633, doi:10.1029/2003JD003550.
- Intergovernmental Panel on Climate Change (2001), *Climate Change*, edited by J. T. Houghton et al., Cambridge Univ. Press, New York.
- Kaufman, Y. J., D. Tanré, and O. Boucher (2002), A satellite view of aerosols in the climate system: Review, *Nature*, *419*, 215–223.
- King, M. D., Y. J. Kaufman, D. Tanré, and T. Nakajima (1999), Remote sensing of tropospheric aerosols from space: Past, present, and future, *Bull. Am. Meteorol. Soc.*, *80*(11), 2222–2259.
- Lacis, A. A., and V. Oinas (1991), A description of the correlated k -distribution method, *J. Geophys. Res.*, *96*, 9027–9064.
- Lelieveld, J., et al. (2002), Global air pollution crossroad over the Mediterranean, *Science*, *298*, 794–799.
- Léon, J.-F., P. Chazette, J. Pelon, F. Dulac, and H. Randriamiarisoa (2002), Aerosol direct radiative impact over the INDOEX area based on passive and active remote sensing, *J. Geophys. Res.*, *107*(D19), 8006, doi:10.1029/2000JD000116.
- Mallet, M., J. C. Roger, S. Despiou, O. Dubovik, and J. P. Putaud (2003), Microphysical and optical properties of aerosol particles in urban zone during ESCOMPTE, *Atmos. Res.*, *69*, 73–97.
- Mallet, M., J. C. Roger, S. Despiou, J. Putaud, and O. Dubovik (2004), A study of the mixing state of black carbon in urban zone, *J. Geophys. Res.*, *109*, D04202, doi:10.1029/2003JD003940.
- Markowicz, K. M., P. J. Flatau, P. K. Quinn, C. M. Carrico, M. K. Flatau, A. M. Vogelmann, D. Bates, M. Liu, and M. J. Rood (2003), Influence of relative humidity on aerosol radiative forcing: An ACE-Asia experiment perspective, *J. Geophys. Res.*, *108*(D23), 8662, doi:10.1029/2002JD003066.
- Mie, G. (1908), Beiträge zur Optik trüber Medien, speziell kolloidaler Metallösungen, *Ann. Phys.*, *25*, 377–445.
- Nakajima, T., et al. (2003), Significance of direct and indirect radiative forcings of aerosols in the East China Sea region, *J. Geophys. Res.*, *108*(D23), 8658, doi:10.1029/2002JD003261.
- Putaud, J. P., et al. (2000), Chemical mass closure and assessment of the origin of the submicron aerosol in the marine boundary layer and the free troposphere at Tenerife during ACE-2, *Tellus, Ser. B*, *52*, 141–168.
- Ramanathan, V., et al. (2001), The Indian Experiment: An integrated assessment of the climate forcing and effects of the great Indo-Asian haze, *J. Geophys. Res.*, *106*, 28,371–28,398.
- Russell, P. B., P. V. Hobbs, and L. L. Stowe (1999), Aerosol properties and radiative effects in the United States East Coast haze plume: An overview of the Tropospheric Aerosol Radiative Forcing Observational Experiment (TARFOX), *J. Geophys. Res.*, *104*, 2213–2222.
- Satheesh, S. K., and V. Ramanathan (2000), Large difference in tropical aerosol forcing at the top of the atmosphere and Earth's surface, *Nature*, *405*, 60–63.
- Satheesh, S. K., V. Ramanathan, X. Li-Jones, J. M. Lobert, I. A. Podgorny, J. M. Prospero, B. N. Holben, and N. G. Loeb (1999), A model for the natural and anthropogenic aerosols over the tropical Indian Ocean derived from Indian Ocean Experiment data, *J. Geophys. Res.*, *104*, 27,421–27,440.
- Scott, N. A. (1974), A direct method of computation of the transmission function of an inhomogeneous gaseous medium—I: Description of the method, *J. Quant. Spectrosc. Radiat. Transfer*, *14*, 691–704.
- Seinfeld, J. H., and S. P. Pandis (1998), *Atmospheric Chemistry and Physics: From Air Pollution to Climate Change*, 2nd ed., 1326 pp., John Wiley, Hoboken, N. J.
- Stamnes, K., S. Tsay, W. Wiscombe, and K. Jayaweera (1988), Numerically stable algorithm for discrete-ordinate-method radiative transfer in multiple scattering and emitting layered media, *Appl. Opt.*, *27*, 2502–2509.
- Tanré, D., L. A. Remer, Y. J. Kaufman, S. Mattoo, P. V. Hobbs, J. M. Livingston, P. B. Russell, and A. Smirnov (1999), Retrieval of aerosol optical thickness and size distribution over ocean from the MODIS airborne simulator during TARFOX, *J. Geophys. Res.*, *104*, 2261–2278.
- van Dingenen, R., J. P. Putaud, A. Dell'Acqua, S. Martins-Dos Santos, J. Viidanoja, and F. Raes (2002), Airborne and ground based aerosol measurements in the Marseille area during ESCOMPTE (June–July 2001), paper presented at the IGAC Conference, Heraklion, Crete.
- Vermote, E. F., N. El Saleous, and C. Justice (2002), Atmospheric correction of the MODIS data in the visible to middle infrared: First results, *Remote Sens. Environ.*, *83*, 1–2, 97–111.
- H. Cachier, Laboratoire des Sciences du Climat et de l'Environnement (LSCE), UMR CEA/CNRS 1572, Bat 12, Avenue de la Terrasse, 91191 Gif-sur-Yvette, France.
- S. Despiou, Laboratoire des Echanges Particulaires aux Interfaces (LEPI), UMR CNRS 6017, Université de Toulon et du Var, BP 132, 83957 La Garde, France.
- O. Dubovik, NASA Goddard Space Flight Center, Code 614.4, Greenbelt, MD 20771, USA.
- P. Dubuisson, Ecosystèmes Littoraux et Côtiers (ELICO), UMR CNRS 8013, Université du Littoral Côte d'Opale, 32 avenue Foch, 62930 Wimereux, France.
- M. Mallet, Laboratoire d'Aérodologie (LA), UMR 5560, Observatoire Midi-Pyrénées, 14 rue Edouard Belin, 31400 Toulouse, France.
- J. C. Roger and E. Vermote, Department of Geography, University of Maryland at College Park, College Park, MD 20742, USA. (jc@ltdri.org)